Extended Use of the Parameter Observer on a Class of Second-Order Systems

Toma-Leonida DRAGOMIR, Dadiana-Valeria CĂIMAN*, Corneliu BĂRBULESCU, Sorin NANU
Department of Automation and Applied Informatics, Politehnica University Timișoara,
2 Vasile Pârvan Blvd., 300223 Timișoara, Romania
toma.dragomir@upt.ro, dadiana.caiman@upt.ro (**Corresponding author*),
corneliu.barbulescu@student.upt.ro, sorin.nanu@upt.ro

Abstract: The paper extends the use of a parameter observer (PO) from first-order to second-order observed systems. A procedure for identifying a linking relationship between the coefficients of a second-order linear system is proposed, based on experiment. The link relation uses link parameters provided by POs from processing the free response of the observed system. By combining the connection relations obtained from several experiments carried out on the system, after the controlled modification of its coefficients, it is possible to calculate the coefficients of the second-order system or the primary parameters that appear in their expressions. The application of the method is illustrated for time-invariant systems. The examples include both tutorial examples and mathematical models of some physical systems. In this context, the suitability of the RLC series circuit as an equivalent model of a capacitor is discussed. The limitations due to the sensitivity of the calculation formulas in relation to the estimation errors of the link parameters, respectively the spectrum of the signal at the PO input, e.g., the voltage at the capacitor terminals, are highlighted.

Keywords: Parameter observer, Linear system, Identification, Capacitor, Equivalent model of capacitor.

1. Introduction

The area of modeling and identification is a topic of continuous interest extended from complex systems to apparently very simple structures. The electric capacitors are examples of such structures. These devices are intended for the implementation of electrical capacities. But, practically, they are physical structures with distributed parameters, whose behavior in electric circuits is not purely capacitive. The capacitors show also resistive and inductive behavior, depending on the frequency. Over time, the capacitive character degrades, and the resistive-dissipative behavior increases. Hence, for reasons such as circuit sizing and maintenance, capacitors are associated with approximate electrical models with lumped parameters, called capacitor equivalent circuits. The topologies of the equivalent circuits associable to capacitors depend on the type of capacitors (e.g., Aluminium electrolytic capacitors (Al-Caps), metallized polypropylene film capacitors (MPPF-Caps) and multilayer ceramic capacitors (MLC-Caps)) and on the working regime to which they are subjected. Frequency characteristics of the parameters of simple series or parallel equivalent circuits can be determined experimentally, using precision measurement bridges or other equipment. The characteristics show important variations related to frequency, which means that the parameters are not constant during the transient regimes. Consequently, the "equivalent" attribute must be associated with both the capacitor type and its operating mode. In these circumstances, the selection of "the right model and the right electrical parameters" is an open research topic (Kareem & Hur, 2022).

Usually, for reasons of simplicity and long practice, the lumped-parameter series RC equivalent model of the capacitor is used. Recently, a PO aimed at obtaining the values of the equivalent parameter of the RC model for an electrolytic capacitor has been proposed and implemented in (Bărbulescu et al., 2022; Bărbulescu et al., 2023). The principle on which PO is based is new in the specialized literature The PO is a discrete time linear dynamic system of the second order. It approximates the time constants of the capacitor discharge circuit across a two-stage variable resistance. The implementation was performed with a microcontroller using a sampling time $h = 20\ \mu s$. The determination of the equivalent parameters of the capacitor was made during its discharge, in less than 25 *ms*. From a systemic point of view, PO approximates the time constant of a first-order system. Hence, it can be used for any physical system that is dynamically described by a mathematical model of the same type as that of the discharge circuit of the electrolytic capacitor.

Another lumped-parameter equivalent model associated with a capacitor is the series RLC structure. The estimation of its parameters requires relatively sophisticated theoretical and practical procedures as observed in (Ren & Gong, 2018). In this context, researching the possibility to use

https://doi.org/10.24846/v32i3y202306

the PO for estimating the equivalent parameters of the RLC model is naturally a subject of interest.

The structure of this paper is organized as follows. Section 2 contains the problem statement and explains the importance of the problem investigated in this paper and the novelty of this research study. Further, in Section 3, two forms of the linking relationship obtained with either continuous or discrete time PO are deduced and, based on numerical examples, it is demonstrated how these relationships can be used to identify the primary parameters of the observed systems. The application of the method for the two models of physical systems represents the subject of Section 4. In the next section, Section 5, aspects related to the theoretical results of the paper and their practical application are outlined. The last section, Section 6, summarizes the contributions of this article.

2. Problem Statement

To carry out the above research, this paper extends the use of PO to second-order linear systems. The extension consists in determining, on the basis of the free response of the system, the value of a link parameter between the coefficients of the system and in establishing a corresponding linking relationship. This relationship can be further used to estimate the coefficients of the observed system or its primary parameters. The "primary" attribute refers to the physical parameters that appear in the expressions of the coefficients of the mathematical model.

The main contribution of this article consists in proposing the mentioned extension and illustrating some possibilities of using it to determine the primary parameters of an electrolytic capacitor and a mechanical system. For the capacitor, the RLC equivalent series model was adopted.

3. Main Results

3.1 Methodology for Identifying and Using a Link Relationship Between the Coefficients of a Second-Order Continuous Time-Varying System Through POs

Consider the second-order unforced dynamic linear system (1), with the properties (2):

$$\begin{aligned} &a_2(t)\cdot\ddot{y}(t)+a_1(t)\cdot\dot{y}(t)+y(t)=0,\\ &y(0)\geq 0,\ \dot{y}(0)<0, \end{aligned} \tag{1}$$

$$y(t)>0,\ \dot{y}(t)<0,\ \ddot{y}(t)>0,\ t>0. \tag{2}$$

The first order time variable systems (3) and (4) are associated to $y(t)$ and to $-\dot{y}(t)$, respectively.

$$a_1^*(t)\cdot\dot{y}(t)+y(t)=0,\ y(0)>0, \tag{3}$$

$$a_2^*(t)\cdot\left[-\ddot{y}(t)\right]+\left[-\dot{y}(t)\right]=0,-\dot{y}(0)>0. \tag{4}$$

Due to restrictions (2), the coefficients $a_1^*(t)$ and $a_2^*(t)$ are defined for $t>0$. Their measurement unit is time, same as for $a_1(t)$ in (3).

Proposition 1. The coefficients $a_1^*(t)$ and $a_2^*(t)$ are related to the coefficients $a_1(t)$ and $a_2(t)$ by the linking equation:

$$a_2(t)-a_1(t)\cdot a_2^*(t)+a_1^*(t)\cdot a_2^*(t)=0,\ t>0. \tag{5}$$

Proof. By subtracting equation (1) from (3), term by term, one obtains:

$$\begin{aligned} &a_2(t)\cdot\left[-\ddot{y}(t)\right]+\left[a_1(t)-a_1^*(t)\right]\cdot\\ &\left[-\dot{y}(t)\right]=0,-\dot{y}(0)>0. \end{aligned} \tag{6}$$

As the system of equations (4) and (6) is consistent with an infinite number of solutions in relation to $\ddot{y}(t)$ and $\dot{y}(t)$, its determinant is 0. Equation (5) is obtained by developing this determinant. This result closes the proof.

This equation represents a link relationship between $a_1(t)$ and $a_2(t)$. In relation with these coefficients, $a_1^*(t)$ and $a_2^*(t)$ play the role of link parameters.

In order to estimate experimentally $a_1^*(t)$ and $a_2^*(t)$ the PO presented in (Bărbulescu et al., 2022) can be used. Since the parameter observer can generate the estimate $-\hat{\dot{y}}(t)$ of the derivative $-\dot{y}(t)$, besides $a_1^*(t)$, a second PO can also be used to estimate $a_2^*(t)$, as it can be seen in Figure 1.

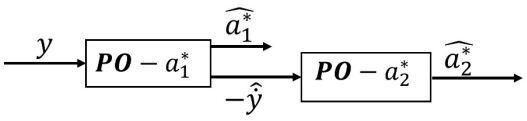

Figure 1. Block diagram of an estimation structure with two POs associated to system (1)

The mathematical model of the structure displayed in Figure 1 is explained at the end of the paper, in Appendix A. As shown in Appendix A, the structure provides the estimates $\widehat{a_1^*}(t)$ and $\widehat{a_2^*}(t)$ only for $t \geq t_0$, t_0 this being the moment when the transients of POs end.

Using them, equation (5) can be approximated as in the link relationship from equation (7), where the validation function $E\left(\widehat{a_1^*}, \widehat{a_2^*}\right)$ is given in (8).

$$E\left(\widehat{a_1^*}, \widehat{a_2^*}\right) = 0, \ t \geq t_0, \tag{7}$$

$$E(\widehat{a_1^*}, \widehat{a_2^*}) = a_2 - a_1 \cdot \widehat{a_2^*}(t) + \widehat{a_1^*}(t) \cdot \widehat{a_2^*}(t). \tag{8}$$

The relationship (8) can be used in various practical contexts. Following the proposed investigation is limited to the case of time-invariant systems when the coefficients in (1) are constant. In this case, the link relationship (7) takes the specific form:

$$a_2 - a_1 \cdot \widehat{a_2^*} + \widehat{a_1^*} \cdot \widehat{a_2^*} = 0, \quad t \geq t_0. \tag{9}$$

Proposition 2. The link parameters $\widehat{a_1^*}(t)$ and $\widehat{a_2^*}(t)$ in equation (9) are equal: $\widehat{a_1^*} = \widehat{a_2^*}$.

Proof. The characteristic polynomial $\mu(r) = a_2 r^2 + a_1 \cdot r + 1$ associated with equation (1) has, due to the conditions (2), two real negative roots r_1 and r_2: $r_1 < r_2 < 0$. Consequently, $y(t)$ has the form (10), with γ_1 and γ_2 depending on $y(0)$ and $\dot{y}(0)$, respectively.

$$y(t) = \gamma_1 \cdot e^{r_1 t} + \gamma_2 \cdot e^{r_2 t}. \tag{10}$$

By a simple calculation, the equality (11) can be deduced. Considering (3) and (4), (11) connects parameters in the form of (12):

$$\lim_{x \to \infty} \frac{y(t)}{\dot{y}(t)} = \lim_{x \to \infty} \frac{\dot{y}(t)}{\ddot{y}(t)} = \frac{1}{r_2}, \tag{11}$$

$$a_1^* = a_2^* = -\frac{1}{r_2}. \tag{12}$$

End of proof.

This result emphasises that it is sufficient to calculate only the link parameter $a_1^*(t)$. Based on Proposition 2, equation (9) becomes:

$$a_2 - a_1 \cdot a_1^* + a_1^{*2} = 0, \quad t \geq t_0 \tag{13}$$

Equation (13) excludes the use of $PO - a_2^*$, $PO - a_1^*$ being enough. This ensures the approximation of a_1^* by $\widehat{a_1^*}$ and r_2 by $-\frac{1}{\widehat{a_1^*}}$. Equation can be replaced by equation (14):

$$a_2 - a_1 \cdot \widehat{a_1^*} + \widehat{a_1^*}^2 = 0, \ t \geq t_0. \tag{14}$$

According to the last equation in (A1) of Appendix 1, one has: $\widehat{a_1^*} = -\hat{c}_1^{-1}$. Considering this, equation (14) becomes:

$$\hat{c}_1^2 \cdot a_2 + \hat{c}_1 \cdot a_1 + 1 = 0, \ t \geq t_0. \tag{15}$$

As the simple PO structure displayed in Figure 2 is sufficient, the last equation in (A1) of Appendix 1 can be cut out.

According to (15) the linking relationship is fulfilled only after t_0 seconds of applying the signal $y(t)$, when the validation function $F(\hat{c}_1)$ from (16) is close to value 0.

$$F(\hat{c}_1) = \hat{c}_1^2 \cdot a_2 + \hat{c}_1 \cdot a_1 + 1. \tag{16}$$

Note that $F(\hat{c}_1)$ is only a simplified version of $E\left(\widehat{a_1^*}, \widehat{a_2^*}\right)$, usable for time-invariant systems.

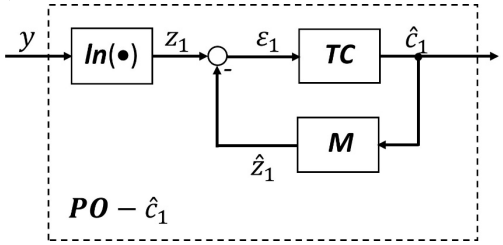

Figure 2. Block diagram of the single PO associated to system

In practical applications, $\hat{c}_1(t)$ is obtained with an observer either off line, by recording $y(t)$, or on line, in real-time, by measuring $y(t)$. In both cases, a homologous discrete-time PO must be used instead of a continuous-time PO. In the quasi-continuity hypothesis (Cao & McCluskey, 2021) the discrete-time PO can be obtained from continuous-time PO (A3) of Appendix 1 by replacing both the integration operations using Euler method and the derivation operation using the backward difference in the equations, like in (Bărbulescu et al., 2022). Practically, this is done by substituting $s = (z-1)/h$ in the transfer functions of the blocks TC and M illustrated in Figure 2. Note that *s* and *z* are operational variables used in the Laplace and *z* transforms, while *h* is the sampling time of discrete-time implementation. Considering this, the following PO (17) will be used, instead of the PO (A3) of Appendix A. The argument *k* is the discrete time corresponding to continuous time $t = k \cdot h$, e.g.: $y[k] = y(k \cdot h)$.

A detailed block diagram of the tracking loop, i.e., the blocks *TC* and *M*, can be found in (Bărbulescu et al., 2022).

$$\begin{aligned} &z_1[k]=\ln\left(y[k]\right),\\ &\hat{z}_1[k]=\hat{z}_1[k-1]+h\cdot\hat{c}_1[k],\ \ \hat{z}_1[0]=\hat{z}_{1o},\\ &\varepsilon_1[k]=z_1[k]-\hat{z}_1[k],\\ &\hat{c}_1[k]=K_{p1}\cdot\left(\varepsilon_1[k]-\varepsilon_1[k-1]\right)+\\ &h\cdot K_{i1}\cdot\varepsilon_1[k-1]+\hat{c}_1[k-1],\ \ \hat{c}_1[0]=\hat{c}_{1o}. \end{aligned} \tag{17}$$

The following part of this subsection addresses the possibility of using formula (15) to determine the parameters of some second-order systems whose unforced dynamic behaviour is described by models (1) and (2). Figure 3 shows two well-known simple systems that meet the above requirements in damped transient regimes. The model (18) is valid for the mechanical system shown in Figure 3(a) while the model (19) is valid for the electrical system displayed in Figure 3(b).

$$\frac{m}{k_r}\cdot\ddot{x}(t)+\frac{k_f}{k_r}\cdot\dot{x}(t)+x(t)=0, \tag{18}$$

$$LC\cdot\ddot{v}(t)+\left(R+R_{ext}\right)\cdot C\cdot\dot{v}(t)+v(t)=0. \tag{19}$$

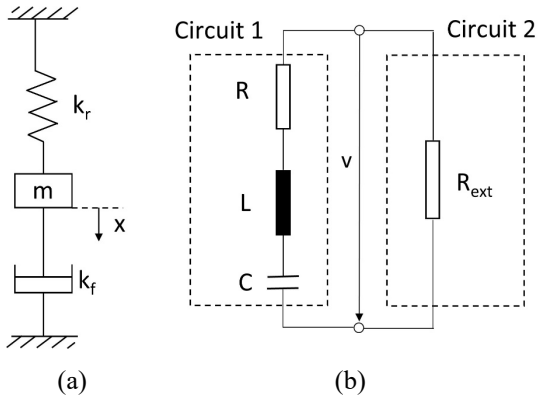

Figure 3. Dynamic systems of the second-order: (a) Mass-spring-damper system; (b) Resistance-inductance-capacitance circuit

The primary parameters of the model (18) are: *m* - the suspended mass, k_r - the spring constant and k_f - the damping factor. The displacement *x* of the mass relative to equilibrium position is measured. This model is a linearized one, around the stationary point. When the system is heavily damped, i.e. $(k_f)^2-4mk_r>0$, the movement of the mass is described by an exponential decaying curve that meets the conditions (2). In (19), the primary parameters R, L, C are the resistance, the inductance and the capacitance of the serial circuit 1, respectively, and R_{ext} is the resistance of circuit 2. It is supposed that circuit 1 is discharged over circuit 2 and the voltage *v* is measured. When $\left(R+R_{ext}\right)^2C-4L>0$, the circuit is heavily damped and meets conditions (2). In both cases, during the estimating process, the values of all the primary parameters, or only of some of them, are considered unknown.

Both models can be considered as having the form (20) for which p_1, p_2 and p_3 represent the triplet of the primary parameters $\{m, k_r, k_f\}$ or $\{R, L, C\}$. The value of R_{ext} is considered known.

$$\begin{aligned} &a_2\left(p_1,p_2,p_3\right)\cdot\ddot{y}(t)+a_1\left(p_1,p_2,p_3\right)\cdot\dot{y}(t)+y(t)=0,\\ &y(0)\geq 0,\dot{y}(0)<0. \end{aligned} \tag{20}$$

With these notations, equation (15) becomes:

$$\hat{c}_1^2\cdot a_2\left(p_1,p_2,p_3\right)+\hat{c}_1\cdot a_1\left(p_1,p_2,p_3\right)+1=0. \tag{21}$$

This equation is able to facilitate the calculation of the values of some parameters p_1, p_2, and p_3 when one or several of those parameters may be changed in a controllable way, by adding new physical components to the original physical structure, and when the expressions of the coefficients a_1 and/or a_2 can capture these changes. As an example, a spring or damper may be added, or an additional resistor may be inserted, all with well-calibrated values. Supposing that, after these double interventions, the parameter p_2 changes to p_2+p_2' respectively to p_2+p_2'', instead of (21), equations (22) and (23) are obtained.

$$\left(\hat{c}_1'\right)^2\cdot a_2\left(p_1,p_2+p_2',p_3\right)+\hat{c}_1'\cdot a_1\left(p_1,p_2+p_2',p_3\right)+1=0, \tag{22}$$

$$\left(\hat{c}_1''\right)^2\cdot a_2\left(p_1,p_2+p_2'',p_3\right)+\hat{c}_1''\cdot a_1\left(p_1,p_2+p_2'',p_3\right)+1=0. \tag{23}$$

In the last three equations, the values of $\hat{c}_1$, $\hat{c}_1'$ and $\hat{c}_1''$ are obtained with the POs (17) or (A1) of Appendix A by performing three unforced dynamical experiments. Equations (21) – (23) represent an algebraic system of 3 equations in 3 parameters p_1, p_2, p_3. If the system is constant, the values of all three parameters are obtained. Obviously, when one of the parameters p_1, p_2 or p_3 is known, equations (21) and (22) are sufficient.

3.2 Numerical Examples

To illustrate how to use the above results in practice, the systems (S_1) and (S_2) of equations (24) and (25) are taken into account. The roots of their characteristic polynomial are given in (26).

$$(S_1): 3\cdot\ddot{y}_1(t)+4\cdot\dot{y}_1(t)+y_1(t)=0,\quad y_1(0)=24,\ \dot{y}_1(0)=-10, \tag{24}$$

$$(S_2): 0.02\cdot\ddot{y}_2(t)+0.3\cdot\dot{y}_2(t)+y_2(t)=0,\quad y_2(0)=0.02,\ \dot{y}_2(0)=-0.1, \tag{25}$$

$$(S_1): r_1=-1<r_2=-\frac{1}{3}<0,\quad (S_2): r_1=-10<r_2=-5<0. \tag{26}$$

The first system is studied using the structure illustrated in Figure 1 while the second one using the structure illustrated in Figure 2.

The transients of (S_1) are illustrated in Figure 4, where the validation function is $E(\cdot,\cdot)=3-4\cdot\widehat{a_2^*}(t)+\widehat{a_1^*}(t)\widehat{a_2^*}(t)$ and the settings of PO are: $\tau=1\,s, \omega_{o1}=10/\tau,\ \omega_{o2}=20/\tau$, $\hat{c}_{o1}=\hat{c}_{o2}=5,\ \hat{z}_{1o}=\hat{z}_{2o}=0.$

The transients of (S_2) are illustrated in Figure 5, where the validation function is $F(\hat{c}_1)=0.02\cdot\hat{c}_1^2(t)+0.3\cdot\hat{c}_1(t)+1$ and the settings of PO are: $\tau=0.1\,s, \omega_o=10/\tau$, $\hat{c}_o=5,\ \hat{z}_o=0.$

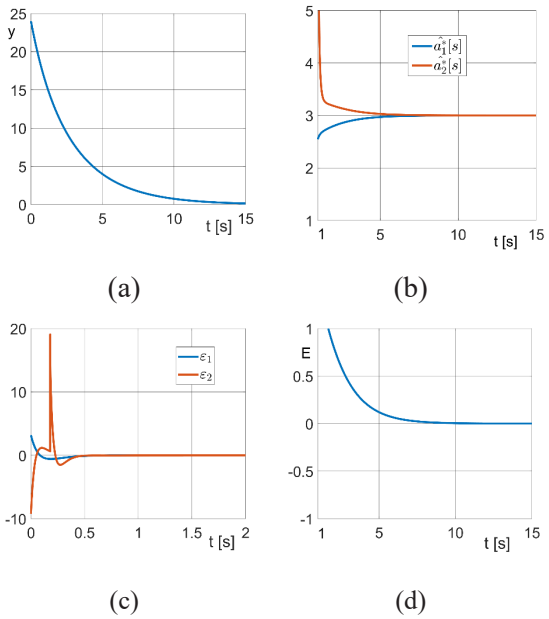

Figure 4. The behavior of the structure from Figure 1 when $y(t)$ is the output signal of system (S_1): (a) the input signal; (b) the estimated link parameters; (c) the tracking errors; (d) the validation function

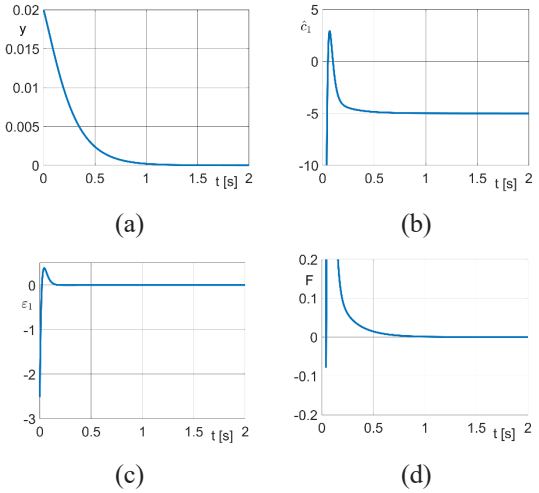

Figure 5. The behavior of the structure from Figure 2 when $y(t)$ is the output signal of system (S_2): (a) the input signal; (b) the estimated link parameter; (c) the tracking error; (d) the validation function

According to equation (7), to Figure 4(d) and Figure 5(d), the link relationships (9) and (14) are not instantaneously fulfilled. Only after t_o' seconds $\widehat{a_1^*}(t)\to 3\,s\quad \widehat{a_2^*}(t)\to 3\,s\quad \hat{c}_1(t)\to -5\,s^{-1}$. It is worth mentioning that the validation functions converge with a delay towards the limit values. It can be considered that for time-invariant case the convergence is practical achieved after $t_0'\cong -4/r_2$ seconds.

4. Simulation Experiments

This section emphasizes, by simulation, the aspects presented in the above subsection, based on two examples. The simulations were performed in MATLAB/Simulink environment.

The scenarios of all experiments are very simple. Free regimes of the systems (18) and (19) are generated for known primary parameters and initial values. The generated signals are processed by the PO illustrated in Figure 2, in order to estimate the values of $\hat{c}_1$. After that, these values are used through link relationships to refine the values of some primary parameters.

Example 1. *Formulation*: The system from Figure 3(a) with the primary parameters $m=0.2\ kg$, $k_r=10\ Nm^{-1}$, $k_f=3\ Nm^{-1}s$ and initial conditions $x(0)=0.02\ m$, $\dot{x}(0)=0\ ms^{-1}$ is considered. The goal is to calculate the values of k_r and k_f from two free responses. The first experiment is performed with the primary

parameters, while, in the second experiment, an additional spring with $k_r^{'} = 1\,Nm^{-1}$ is added, in parallel with the original one.

Results: For both experiments, the recordings lasted 2 *s* and the sampling time was $h = 5 \cdot 10^{-3}\,s$. By proceeding in the same way as in the case of system (18), PO leads to $c_1 = -5\,s^{-1}$, for the first experiment, and to $\hat{c}_1^{'} = -6.36537\,s^{-1}$, for the second one.

In order to find the values of k_r and k_f, *m* and are considered known, and the equation (27) obtained by customizing the equations (21) and (22) is solved.

$$\begin{bmatrix} 1 & \hat{c}_1 \\ 1 & \hat{c}_1^{'} \end{bmatrix} \cdot \begin{bmatrix} k_r \\ k_f \end{bmatrix} = \begin{bmatrix} -\hat{c}_1^2 \cdot m \\ -\left(\hat{c}_1^{'}\right)^2 \cdot m - k_r^{'} \end{bmatrix}. \tag{27}$$

The results are $k_r = 10.02737704\,Nm^{-1}$, $k_f = 3.005475407\,Nm^{-1}$. Note that, relative to the initial values of primary parameters, in this example both errors found are below 0.3%.

Example 2. *Formulation*: Consider the system from Figure 3(b) with the primary parameters $R = 0.684\,\Omega$, $L = 10^{-8}\,H$, $C = 470 \cdot 10^{-6}\,F$ for the branch 1, $R_{ext1} = 19.39\,\Omega$ for the branch 2, and the initial conditions $v(0) = 24\,V$ and $\dot{v}(0) \in \{-2500\,Vs^{-1}, -5000\,Vs^{-1}, -7500\,Vs^{-1}\}$. The aim is to obtain the parameters of circuit 1 by running 3 experiments in free regime. The first experiment is performed with the primary parameters. In the second and the third experiment, the value of resistance R_{ext} was modified to $R_{ext2} = 9.39\,\Omega$ and $R_{ext3} = 6.062\,\Omega$, respectively.

Results: The recordings for the experiments were performed for an interval of 2 *s*. Both continuous time PO and discrete time PO ($h = 20 \cdot 10^{-6}\,s$) were used. The results were very close. Thus, by using the continuous time PO the following values were obtained after three discharge processes: $\hat{c}_1 = -105.99081831307344669\,s^{-1}$, $\hat{c}_1^{'} = -211.2030991176408704\,s^{-1}$ and $\hat{c}_1^{''} = -315.3958733989165746\,s^{-1}$. To refine from these the values of R, L and C, assuming that only the values R_{ext}, $R_{ext}^{'}$ and $R_{ext}^{''}$ were known, equations (21) – (23) were customized, in the following form (28):

$$\begin{bmatrix} \hat{c}_1^2 & \hat{c}_1 & \hat{c}_1 \cdot R_{ext} \\ \left(\hat{c}_1^{'}\right)^2 & \hat{c}_1^{'} & \hat{c}_1^{'} \cdot R_{ext}^{'} \\ \left(\hat{c}_1^{''}\right)^2 & \hat{c}_1^{''} & \hat{c}_1^{''} \cdot R_{ext}^{''} \end{bmatrix} \cdot \begin{bmatrix} LC \\ RC \\ C \end{bmatrix} = \begin{bmatrix} -1 \\ -1 \\ -1 \end{bmatrix}. \tag{28}$$

After solving this system, one obtains:

$$\begin{aligned} &R = 0.6839998955181 56\,\Omega, \\ &L = 9.669632620322943 \cdot 10^{-9}\,H, \\ &C = 470.0000016246609 \cdot 10^{-6}\,F. \end{aligned} \tag{29}$$

It can be noticed that, this time, the values of primary parameters were approximated with an accuracy of 3.35% for *L*, and with an accuracy of less than 0.0001% for *R and C.*

5. Discussion

The coefficients of second-order system (1) can be combined through the link relationship (5). The system can be identified by obtaining the link parameters $a_1^*(t)$ and $a_2^*(t)$ as outputs of the system with the two POs illustrated in Figure 1, when the free response $y(t)$ of the system is applied to its input. If the system (1) is time invariant, its coefficients can be combined through the simpler relationship (15), where the link parameter $\hat{c}_1$ is obtained as the output of the PO illustrated in Figure 2. The values of the link parameters are not established instantly, but only after the end of a transient regime. This is due to the initialization of the PO and the signal generated by the system (1). For the structures shown in Figure 1 and Figure 2, both continuous-time PO and discrete-time PO can be used.

If (1) is the model of a time-invariant physical system with three primary parameters, then equation (20) corresponds to equation (1). By changing the values of the primary parameters in a controlled manner, e.g., with quantities of known values, the obtained link relationships generate an algebraic system of equations whose solving provides the initial values of the primary parameters.

The result in (29) although spectacular, must be viewed with circumspection. The voltage values were obtained by simulation, the estimation of link parameters with PO was performed in double precision, and the results were rendered with many decimal digits. If the voltage was obtained by measurement, the precision of the link parameter

values would be lower than that obtained by simulation, since the signal would be affected by measurement noises. As a result, the number of correct decimal digits of the values of $\hat{c}_1$, $\hat{c}_1^{'}$ and $\hat{c}_1^{''}$ provided by PO is lower. The effect of the truncation of these coefficients on the calculated values of the primary parameters R, L, C depends on the sensitivity of the calculation formulas resulting by solving the system (28). Through several numerical cases, Table 1 highlights the effect of altering the $\hat{c}_1$, $\hat{c}_1^{'}$ and $\hat{c}_1^{''}$ values.

Table 1. The effect of altering the values of link parameters $\hat{c}_1$, $\hat{c}_1^{'}$ and $\hat{c}_1^{''}$ on the values of the primary parameters R, L, C

$\Delta\hat{c}_1[\%]$	0	8,201e-08	-7,843e-06
$\Delta\hat{c}_1^{'}[\%]$	0	3,899e-08	-4,317e-06
$\Delta\hat{c}_1^{''}[\%]$	0	1,619e-08	-1,077e-06
$\Delta R[\%]$	-1,52e-05	-1,31e-05	-1,309 e-04
$\Delta L[\%]$	-3.303	-3,110	-5,767
$\Delta C[\%]$	3.456e-07	2,000e-07	1,200e-05

The first column corresponds to the values in (29). The percentages in the first three rows are calculated in relation to the values in (29), and those in the last three rows in relation to $R = 0.684\,\Omega,\ L = 10^{-8}\,H,\ C = 470 \cdot 10^{-6}\,F$. Note that the sensitivity of estimated values in relation to the altered values is very high for L, low for R and very low for C.

Consequently to practically determine the equivalent values of the primary parameters of the circuit illustrated in Figure 3(b), by using a PO, a prior sensitivity study is required to provide the admissible variation ranges for $\hat{c}_1$, $\hat{c}_1^{'}$ and $\hat{c}_1^{''}$. The conclusion is valid for all systems of type (20). The way the study is carried out depends on the $a_2(p_1, p_2, p_3)$ and $a_1(p_1, p_2, p_3)$ expressions.

Next, the discussion will focus on the issue of the serial RLC model of a capacitor, raised by the second example mentioned above, in the previous section. The subject of capacitor modeling has been topical for a long time, as described in (Keysight Technologies, 2020). Many aspects at different levels of depth are found in the last 5 years researches. In (Kovacs et al., 2018), the general model of a capacitor (Figure 6(a)) is compared with more complex models for Al-Caps capacitor types. Liu et al. (2020) use the general model, and a more complex one developed from it, for modelling the aging process of MPFF-Caps capacitor. In the review (Dang & Kwak, 2020), regarding all three types of capacitors mentioned in the introductory section of this article, the simplified equivalent model from Figure 6(b) and the RC series model from Figure 6(c) is used.

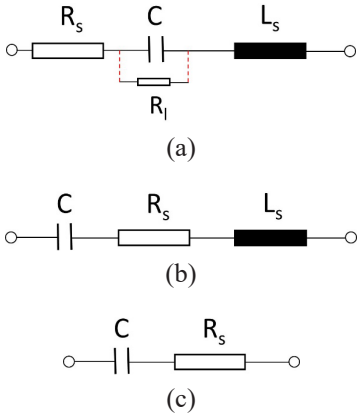

Figure 6. Some electrical models of a capacitor: (a) General model; (b) Simplified equivalent model; (c) The RC series model

The models illustrated in Figure 6(a) and Figure 6(b), together with other newer models derived from the general one, are used in (Plazas-Rosas et al., 2021) with reference to Al-Caps for DC-link capacitor diagnosis. A method for identifying the parameters of the equivalent model displayed in Figure 6(c), of a non-solid Al-Caps considered as an approximation model of a more complex electrical scheme, is presented in (Yang et al., 2022). Determining the physical meaning of the parameters for any equivalent scheme requires special care. In this case, a relevant example can be represented by the discussions addressed in (QuadTech, 2003) regarding the R_s parameter from Figure 6(b), and Figure 6(c).

In this context and considering that the voltage variation at the terminals of a capacitor during discharging across an external resistance has the form illustrated in Figure 6(a), the following question appears: Can a model equivalent to the one illustrated in Figure 6(b) be identified by using PO, for a real RLC series capacitor? Since the application of the identification procedure is associated with the discussed sensitivity problems, the limitations are due either to the location of

the spectrum of $v(t)$ in relation to the frequency characteristic of the impedance z of the capacitor and the measurement quality of $v(t)$, or to the inadequacy of the RLC model to the actual behavior of the capacitor. Thus, assuming that the RLC model is adequate and that the R, L, C parameters do not depend on the frequency, the impedance modulus of the capacitor has the expression (30) and the graph in Figure 7.

$$z(f)=\sqrt{R_s^2+\left(2\pi fL_s-\frac{1}{2\pi fC}\right)^2}. \qquad (30)$$

In (30) f is the frequency. The module $z(f)$ has the minimum value R_s for the resonant frequency $f_o=1/\left(2\pi\sqrt{L_sC}\right)$. As mentioned in the paper (Niu et al., 2018) and in the note (Nippon Chemi-Con Corporation, n. d.), usual, $f_o\in\left[5\cdot10^3,10^6\right]Hz$ for Al-Caps, $f_o\in\left[5\cdot10^5,5\cdot10^7\right]Hz$ for MPPF-Caps and $f_o\in\left[10^7,10^9\right]Hz$ for MLC-Caps. In domains I, II and III, the capacitor has, predominantly, a capacitive, a resistive and an inductive behavior, respectively. Consequently, in different operating regimes, the behavior of the capacitor can be manifested by one or more of these behaviors, depending on the spectrum of $v(t)$. This explains the frequent use of the RC model displayed in Figure 6(c), for low and medium frequency signals.

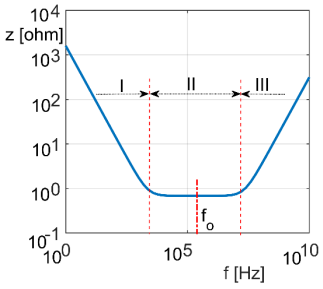

Figure 7. The characteristic $z(f)$ of the impedance from Figure 6(b), for the parameters used in Example 2

The estimation of the values of the parameters C, R and L_s from the signal $v(t)$ assumes that its spectrum has non-negligible values in each of the domains I, II and III, and, in the domains where the amplitudes of the spectrum are small, the ratio signal/noise is favourable.

In the experiments performed, an Al-Caps capacitor of $100\,\mu F/35\,V$ was discharged, having the $z(f)$ characteristic illustrated in Figure 8(a), across three resistors of $50\,\Omega$, $33.33\,\Omega$ and $25\,\Omega$, respectively. For the last case, the amplitude spectrum of the signal $v(t)$ in the discharge process is shown in Figure 8(b).

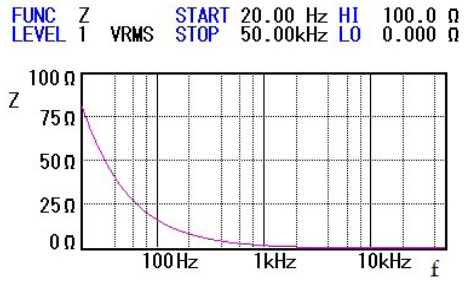

(a)

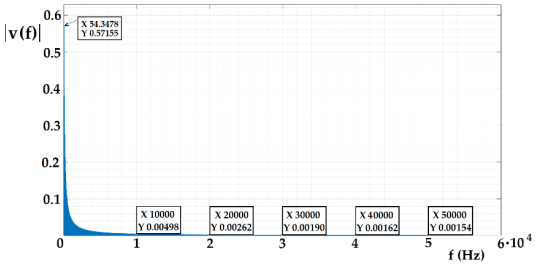

(b)

Figure 8. Characteristics regarding Al-Caps capacitor: (a) $z(f)$ characteristic; (b) Amplitude spectrum of the voltage

For the other two cases, the spectra show insignificant differences compared to this one.

It can be observed that for $f\geq10^4\,Hz$, the amplitudes have negligible values. As a result, it is not surprising that when using the PO only the value of C was well calculated and the values of the other two parameters were often negative.

6. Conclusion

The present work extends the use of the PO proposed by Bărbulescu et al. (2022), from first-order linear systems, to second-order linear systems. With the help of two interconnected POs, the extension consists in determining the values of two link parameters which link the coefficients of the second-order system. When the second-order system represents the model of a physical system, the values of the link parameters can be determined online, with a microcontroller connected to the output of the physical system. If the system is time-invariant, the extension uses a single PO, a link relationship in which a single link parameter appears, respectively.

As the coefficients of the physical system models are functions of the primary parameters of the systems, the link relationship interconnects the primary parameters. By performing several experiments for controlled changes of the primary parameters, it is possible to obtain an algebraic system of equation with the initial values as variables. The expressions of primary parameters obtained by solving the system can be very sensitive in terms of coefficients. In this context, the article reveals and analyses the possibility of identifying the primary parameters of the RLC series equivalent model of a capacitor, by measuring the voltage at the terminals of the capacitor during its discharge over a resistor. Identifying such an equivalent model remains, in the general way, an open problem.

Appendix A

Based on (Bărbulescu et al., 2022), the structure illustrated in Figure 1 is obtained following three steps:

Step 1: The *PO*- a_1^* is associated with the virtual system (3) to estimate a_1^* via $\widehat{a_1^*}(t)$:

$PO-a_1^*$:

$$\begin{cases} z_1(t)=ln\big(y(t)\big), \\ \dfrac{d\hat{z}_1(t)}{dt}=\hat{c}_1(t),\ \hat{z}_1(0)=\hat{z}_{1o}, \\ \varepsilon_1(t)=z_1(t)-\hat{z}_1(t), \\ \hat{c}_1(t)=K_{p1}\varepsilon_1(t)+K_{i1}\int_0^t\varepsilon_1(\tau)d\tau+\hat{c}_{1o}, \\ \widehat{a_1^*}(t)=-\dfrac{1}{\hat{c}_1(t)}. \end{cases} \quad \text{(A1)}$$

The equations in (A1) correspond to $ln(\cdot)$, to M_1, *summation block*, and to TC_1 *and* $-(\cdot)^{-1}$ blocks, respectively, as displayed in Figure A1, where the block marked with "-1" is a polarity inverter.

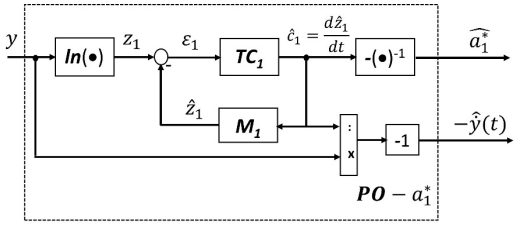

Figure A1. The block diagram of extended *PO*- a_1^*

Step 2: Because $\varepsilon_1(t)\to 0$, $\hat{c}_1(t)\cong c_1(t)$ and $\dot{y}(t)=y(t)\cdot c_1(t)\cong y(t)\cdot\hat{c}_1(t)$, respectively, $\dot{y}(t)$ is approximated by its estimate $\hat{\dot{y}}(t)$ calculated with (A2), and *PO*- a_1^* is extended by means of this operation, as shown in Figure A1.

$$-\hat{\dot{y}}(t)=-y(t)\cdot\hat{c}_1(t) \quad \text{(A2)}$$

Step 3: Considering the system displayed in Figure A1, the *PO*- a_2^* corresponding to system is attached to the output $-\hat{\dot{y}}(t)$. This leads to the structure illustrated in Figure 1, having the equations (A3).

$$\begin{cases} PO-a_1^*:\ \begin{cases}(A1)\\(A2)\end{cases} \\ PO-a_2^*:\ \begin{cases} z_2(t)=ln\big(-\hat{\dot{y}}(t)\big), \\ \dfrac{d\hat{z}_2}{dt}=\hat{c}_2(t),\ \hat{z}_2(0)=\hat{z}_{2o}, \\ \varepsilon_2(t)=z_2(t)-\hat{z}_2(t), \\ \hat{c}_2(t)=K_{p2}\varepsilon_2(t)+K_{i2}\int_0^t\varepsilon_2(\tau)d\tau+\hat{c}_{2o}, \\ \widehat{a_2^*}(t)=-\dfrac{1}{\hat{c}_2(t)}. \end{cases} \end{cases} \quad \text{(A3)}$$

The tracking regime of the asymptotically stable system (A3) is not established instantly, but only after a certain time t_0 when $\widehat{a_1^*}(t)\to\hat{a}_1(t)$ and $\widehat{a_2^*}(t)\to\hat{a}_2(t)$. Consequently, instead of ideal linking relationship (5) one obtains:

$$a_2(t)-a_1(t)\cdot\widehat{a_2^*}(t)+\widehat{a_1^*}(t)\cdot\widehat{a_2^*}(t)=0,\ t\ge t_0 \quad \text{(A4)}$$

In order to extend the tracking time interval of the virtual parameters $\hat{a}_1(t)$ and $\hat{a}_2(t)$, the gains of the two PI tracking controllers need to be matched, according to (A5) and (A6).

$$\omega_{o1}\ge\frac{10}{\tau},\ \omega_{o2}\ge\frac{20}{\tau},\ \omega_{o2}>\omega_{o1}, \quad \text{(A5)}$$

$$K_{p1,2}=2\cdot\omega_{01,2},\quad K_{i1,2}=\omega_{o1,2}^2\ . \quad \text{(A6)}$$

Here is the expected duration of the transients of $\left(PO-a_1^*\right)$. Basically, it can be considered that $t_0=2\cdot\tau$. By adopting ω_{o1} and ω_{o2} as in (A5), the $PO-a_2^*$ will operate "slightly faster" than $PO-a_1^*$.

REFERENCES

Bărbulescu, C., Căiman, D.-V. & Dragomir, T.-L. (2022) Parameter Observer Useable for the Condition Monitoring of a Capacitor. *Applied Sciences*. 12(10): 4891. doi: 10.3390/app12104891.

Bărbulescu, C., Căiman, D.-V., Nanu, S. & Dragomir, T.-L. (2023) Implementation of Parameter Observer for Capacitors. *Sensors*. 23(2): 948. doi: 10.3390/s23020948.

Cao, J. & McCluskey, A. (2021) Topological transitivity in quasi-continuous dynamical systems. *Topology and its Applications*. 301: 107496. doi: 10.1016/j.topol.2020.107496.

Dang, H. L. & Kwak, S. (2020) Review of health monitoring techniques for capacitors used in power electronics converters. *Sensors*. 20(13): 3740. doi: 10.3390/s20133740.

Kareem, A. B. & Hur, J. W. (2022) Towards Data-Driven Fault Diagnostics Framework for SMPS-AEC Using Supervised Learning Algorithms. *Electronics*. 11(16): 2492. doi: 10.3390/electronics11162492.

Keysight Technologies. (July 2020) *Impedance Measurement Handbook – A Guide to Measurement Technology and Techniques.* https://www.keysight.com/us/en/assets/7018-06840/application-notes/5950-3000.pdf [Accessed 17th March 2023].

Kovacs, L., Kohlrusz, G., Enisz, K. & Fodor, D. (2018) Aluminium electrolytic capacitor model for capacitor materials structure transformation analysis in PWM applications. In: *2018 IEEE 18th International Power Electronics and Motion Control Conference (PEMC), 26-30 August 2018, Budapest, Hungary*. Manhattan, New York, USA, Institute of Electrical and Electronics Engineers (IEEE). pp. 888-893. doi: 10.1109/EPEPEMC.2018.8521909.

Liu, H., Vandenbosch, G. A., Claeys, T. & Pissoort, D. (2020) A novel full-parameter ageing modelling approach for capacitors based on complex impedance analysis. *IEEE Transactions on Dielectrics and Electrical Insulation*. 27(3), 980-988. doi: 10.1109/TDEI.2019.008542.

Nippon Chemi-Con Corporation. (n. d.) *Aluminum electrolytic capacitor Frequency Characteristics of Impedance.* https://www.chemi-con.co.jp/en/faq/detail.php?id=alFreqCh [Accessed 17th March 2023].

Niu, H., Wang, S., Ye, X., Wang, H. & Blaabjerg, F. (2018) Lifetime prediction of aluminum electrolytic capacitors in LED drivers considering parameter shifts. *Microelectronics Reliability*. 88-90, 453-457. doi: 10.1016/j.microrel.2018.06.027.

Plazas-Rosas, R. A., Orozco-Gutierrez, M. L., Spagnuolo, G., Franco-Mejía, É. & Petrone, G. (2021) DC-link capacitor diagnosis in a single-phase grid-connected PV system. *Energies*. 14(20): 6754. doi: 10.3390/en14206754.

QuadTech. (July 2003) *Equivalent Series Resistance (ESR) of Capacitors. Application Note*. https://web.archive.org/web/20130916071935/http:/lowesr.com/QT_LowESR.pdf [Accessed 17th March 2023].

Ren, L. & Gong, C. (2018) Modified hybrid model of boost converters for parameter identification of passive components. *IET Power Electronics.* 11(4), 764-771. doi: 10.1049/iet-pel.2017.0528

Yang, Z., Xi, L., Zhang, Y. & Chen, X. (2022) An Online Parameter Identification Method for Non-Solid Aluminum Electrolytic Capacitors. *IEEE Transactions on Circuits and Systems II: Express Briefs*. 69(8), 3475-3479. doi: 10.1109/TCSII.2022.3158938.